J. Fluid Mech. (2010), *vol.* 665, *pp.* 457–479.
doi:10.1017/S002211201000412X

A multimodal method for liquid sloshing in a two-dimensional circular tank

ODD M. FALTINSEN† AND ALEXANDER N. TIMOKHA

Centre for Ships and Ocean Structures and Department of Marine Technology, Norwegian University of Science and Technology, NO-7091 Trondheim, Norway

(Received 25 November 2009; revised 23 July 2010; accepted 2 August 2010; first published online 22 October 2010)

Two-dimensional forced liquid sloshing in a circular tank is studied by the multimodal method which uses an expansion in terms of the natural modes of free oscillations in the unforced tank. Incompressible inviscid liquid, irrotational flow and linear free-surface conditions are assumed. Accurate natural sloshing modes are constructed in an analytical form. Based on these modes, the 'multimodal' velocity potential of both steady-state and transient forced liquid motions exactly satisfies the body-boundary condition, captures the corner-point behaviour between the mean free surface and the tank wall and accurately approximates the free-surface conditions. The constructed multimodal solution provides an accurate description of the linear forced liquid sloshing. Surface wave elevations and hydrodynamic loads are compared with known experimental and nonlinear computational fluid dynamics results. The linear multimodal sloshing solution demonstrates good agreement in transient conditions of small duration, but fails in steady-state nearly-resonant conditions. Importance of the free-surface nonlinearity with increasing tank filling is explained.

Key words: waves/free-surface flows, wave–structure interactions

1. Introduction

Sloshing must be considered for almost any moving vehicle or structure containing a liquid with a free surface and can be the result of both transient and resonant excitations of the tank. The hydrodynamics of sloshing is complicated, depending on the tank shape, liquid depth and the forcing conditions. Its understanding requires a combination of theory, computational fluid dynamics (CFD) and experiments. We must distinguish from a physical point of view between global flow and local flow associated with impact between the free surface and the tank structure. The present paper concentrates on the global flow and the resulting hydrodynamic loads due to forced two-dimensional transverse liquid sloshing in a circular-shaped tank. The latter is needed in predicting the dynamics of vehicles and structures relevant, for instance for wave liquid motions in lorry tanks, horizontal cylindrical ship tanks, railway cisterns and storage containers exposed to seismic excitations.

Experiments and CFD simulations of two-dimensional forced liquid sloshing in circular tanks are, for instance, reported by Strandberg (1978), Kobayashi *et al.* (1989), Aliabadi, Johnson & Abedi (2003), Djavareshkian & Khalili (2006), Moderassi-Tehrani, Rakheja & Sedaghati (2006), Karamanos, Papaprokopiou &

† Email address for correspondence: oddfal@marin.ntnu.no

Platyrrachos (2009) and Bogomaz & Sirota (2002). To the authors' knowledge, analytical methods, in general, and multimodal methods, in particular, are not presented in the literature for this tank shape.

The multimodal methods have been extensively elaborated for upright circular, annular and sectored cylindrical tanks, for two-dimensional and three-dimensional rectangular tanks. These methods employ a Fourier-type expansion in terms of the natural sloshing modes so that the forced liquid motions are described by the so-called modal equations, i.e. ordinary differential equations coupling generalized coordinates of the free-surface elevations. The fact that analytical natural modes exist for the aforementioned tank shapes provides exact expressions for the hydrodynamic coefficients of the modal equations.

An advantage of the multimodal methods relative to CFD is their central processing unit (CPU)-time efficiency. The latter fact allows for systematic parameter variations. The methods can give accurate results for hydrodynamic characteristics and loads within the theoretical assumptions, and, thereby, be used for validation of CFD results when the assumptions of the modal method about irrotational flow of an incompressible fluid with single-valued free-surface elevations are applicable. Analysing the structure of the modal equations and their solutions simplifies studies of energy distribution between the natural modes. For nonlinear modal equations, we can also analyse transfer of energy between sloshing modes, jumps between steady-state solution branches and hydrodynamic instability.

Even though the general scheme of the multimodal methods is well known from the literature (see e.g. the textbook by Faltinsen & Timokha 2009), their applicability has been demonstrated only for a limited number of tank shapes. Each individual tank shape requires a dedicated applied mathematical and physical study. Specifically, the linear and nonlinear multimodal methods need an accurate approximation of the natural sloshing modes which should exactly satisfy the Laplace equation (constraint I) and zero-Neumann boundary condition on the wetted tank surface (constraint II). Ideally, the natural sloshing modes should be found in an analytical form (constraint III).

The present paper focuses on a multimodal analytical description of the linear forced liquid sloshing and associated hydrodynamic characteristics for a two-dimensional circular tank. The main assumptions are potential flow of an incompressible liquid with small-magnitude tank excitations and linear free-surface conditions. The latter conditions are relevant for the global flow in a clean tank without resonant wave amplification. However, it is believed that an extension of the constructed linear multimodal scheme to nonlinear resonant sloshing can be developed in the spirit of the nonlinear multimodal approach (see details in Faltinsen & Timokha 2009, chapters 8 and 9, and the discussion in § 5).

In § 2, we start with the boundary value problem on linear forced two-dimensional liquid sloshing in a circular tank, and derive all the required expressions of the linear multimodal theory for this tank shape. The derivation is based on the general multimodal solution yielding the so-called linear modal equations, i.e. ordinary differential equations with respect to the generalized coordinates of the free-surface elevations. Modal expressions for computing hydrodynamic characteristics and loads are also derived. They involve the above-mentioned generalized coordinates and small-magnitude three-degrees-of-freedom forcing of the tank.

Bearing in mind the constraints I, II and III, we construct in § 3 an accurate analytical approximation of the natural sloshing modes by means of the Trefftz method. The Trefftz method employs two families of analytical trial functions and

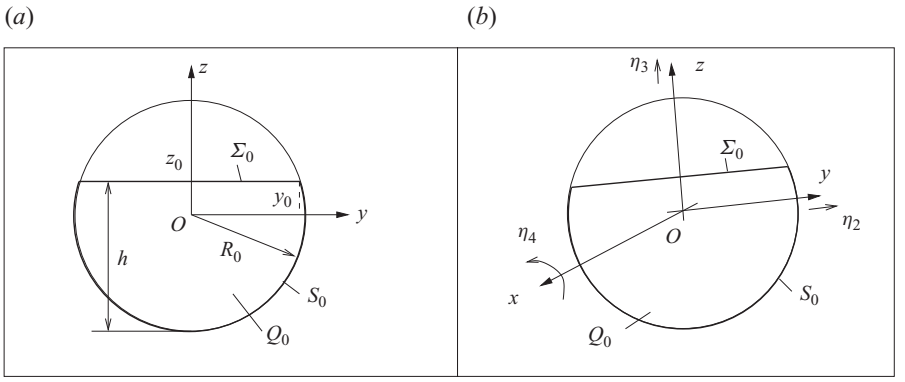

FIGURE 1. Sketch of a two-dimensional circular tank partly filled by a liquid. (*a*) Unperturbed (hydrostatic) shape of the liquid. (*b*) Main definitions for linear liquid sloshing in a tank performing small-magnitude motions associated with translatory (η_2, η_3) and angular (η_4) motions. Liquid sloshing is described in the tank-fixed coordinate system Oyz whose origin O coincides with the centre of the circle.

provides full agreement with benchmark calculations by McIver (1989) for the natural sloshing frequencies. A novelty is that the Trefftz natural sloshing modes capture the corner-point asymptotics between the mean free surface and circular wall and, thereby, effectively approximate the spectral boundary condition in a uniform metric. Requirement in accounting for the singular behaviour is stated for middle and higher depths, i.e. the liquid depth-to-radius ratios $1.0 \lesssim h/R_0 < 2$. To the authors' knowledge, the literature does not give examples of the natural sloshing modes to compare with. However, we show that our results are consistent with the 'high spot' results by Kulczycki & Kuznetsov (2009) which state that the maximum wave elevation associated with a natural mode does not occur at the tank wall for $h/R_0 > 1$.

Using these natural modes facilitates high accuracy of the multimodal solution as discussed in § 2. Laterally forced tank motions are studied in detail and free-surface elevation and horizontal hydrodynamic force which follow from this multimodal solution are compared in § 4 with known experimental and nonlinear CFD simulations with a primary focus on non-resonant conditions. Steady-state sloshing due to a harmonic lateral excitation and transient sloshing associated with the turning and lane change of a tanker vehicle are considered. As long as the tank filling is low, $h/R_0 \lesssim 0.8$, we establish good agreement provided by a clearly dominant contribution of the lowest natural mode. There is an increasing discrepancy with increasing depth in the range $0.8 \lesssim h/R_0 < 2$. Because our linear multimodal solution gives an accurate approximation of the original linear sloshing problem, the discrepancy indicates failure of linear sloshing theory. We discuss different arguments in favour of this point following from the present study and the related literature.

2. Multimodal solution

2.1. *Statement of the problem*

We consider forced linear transversal waves in a horizontal circular cylindrical tank, in the present paper termed a two-dimensional liquid sloshing in a circular tank of radius R_0. In its unperturbed state, the contained liquid occupies the two-dimensional domain, Q_0, with the free surface, Σ_0, as shown in figure 1(*a*). The horizontal

cylindrical tank performs two-dimensional motions in the Oyz-plane which are governed by the small-magnitude translatory velocity $\boldsymbol{v}_O = (0, v_{Oy}, v_{Oz}) = (0, \dot{\eta}_2, \dot{\eta}_3)$, and angular perturbations (around the Ox-axis, roll) with the instant angular velocity $\boldsymbol{\omega} = (\omega_1, 0, 0) = (\dot{\eta}_4, 0, 0)$ depicted in figure 1(b). The two-dimensional sloshing is considered in the tank-fixed coordinate system Oyz with origin at the centre of the circle.

The absolute liquid velocity $\boldsymbol{v}_a = (0, v, w)$ is described by the velocity potential $\Phi(y, z, t)$ ($\boldsymbol{v}_a = \nabla\Phi = (0, \partial\Phi/\partial y, \partial\Phi/\partial z)$). The corresponding boundary value problem (see Faltinsen & Timokha 2009, and other textbooks) is formulated with respect to Φ and small vertical displacements of the free surface presented by the equation $z = \zeta(y, t)$:

$$\frac{\partial^2\Phi}{\partial y^2} + \frac{\partial^2\Phi}{\partial z^2} = 0 \quad \text{in } Q_0, \tag{2.1a}$$

$$\frac{\partial\Phi}{\partial n} = \dot{\eta}_2 n_2 + \dot{\eta}_3 n_3 \quad \text{on } S_0, \tag{2.1b}$$

$$\frac{\partial\Phi}{\partial z} = \dot{\eta}_3 + \dot{\eta}_4 y + \frac{\partial\zeta}{\partial t} \quad \text{on } \Sigma_0, \tag{2.1c}$$

$$\frac{\partial\Phi}{\partial t} + g\zeta + gy\eta_4 = 0 \quad \text{on } \Sigma_0, \tag{2.1d}$$

$$\int_{\Sigma_0} (\zeta - z_0)\,\mathrm{d}S = 0. \tag{2.1e}$$

Here, g is the acceleration due to gravity, $\boldsymbol{n} = (0, n_2, n_3)$ is the outer normal, equation $z = z_0$ determines the mean free surface Σ_0 in the Oyz-coordinate system, y_0 is the half-length of Σ_0 and S_0 is the tank surface below Σ_0. These and other geometric notations are illustrated in figure 1.

Equation (2.1e) implies conservation of the two-dimensional liquid volume (area)

$$|Q_0| = \int_{Q_0} \mathrm{d}Q = R_0^2 \left(\frac{1}{2}\pi + \bar{z}_0\sqrt{1 - \bar{z}_0^2} + \arcsin(\bar{z}_0) \right), \quad \bar{z}_0 = \frac{z_0}{R_0}. \tag{2.2}$$

Because the origin O coincides with the centre of the circle, the body-boundary condition (2.1b) does not include forcing terms associated with the angular tank motion around Ox. The corresponding η_4 terms appear only in the kinematic (2.1c) and dynamic (2.1d) conditions. Appearance of these terms is associated with the fact that the coordinate system is rigidly fixed with the tank and does not cause sloshing. Indeed, using a substitution which accounts for the inclination of the tank-fixed coordinate system,

$$\zeta(y, t) := \zeta(y, t) - \eta_4(t)\, y, \tag{2.3}$$

in the kinematic and dynamic conditions eliminates the angular perturbation from the mathematical statement (2.1). This means that the angular perturbations do not influence the velocity potential Φ.

2.2. *Multimodal solution and linear modal equations*

The idea of multimodal methods (Lukovsky, Barnyak & Komarenko 1984; Faltinsen & Timokha 2009) consists of reducing the evolution problem (2.1) to a system of ordinary differential equations with respect to generalized coordinates responsible for the free-surface elevations. Any small-amplitude tank motions can be considered and both complex transient waves and steady-state regimes can be described.

Henceforth, we consider the following linear multimodal solution of the original boundary problem (2.1):

$$\zeta(y,t) = z_0 - y\eta_4(t) + \sum_{i=1}^{\infty} \beta_i(t)\bar{f}_i(y), \tag{2.4a}$$

$$\Phi(y,z,t) = \dot{\eta}_2(t)y + \dot{\eta}_3(t)z + \sum_{n=1}^{\infty} R_n(t)\bar{\varphi}_n(y,z), \tag{2.4b}$$

where we account for inclination of the tank-fixed coordinate system (see substitution (2.3)) and the fact that the angular perturbations do not affect the absolute velocity field; $\beta_i(t)$ and $R_n(t)$ are generalized coordinates, $\bar{\varphi}_n$ are the normalized natural sloshing modes ($\bar{f}_i(y) = \bar{\varphi}_i(y, z_0)$).

Postulating (2.4), we implicitly assume that the natural sloshing modes are known. The natural sloshing modes φ_i are eigenfunctions of the spectral boundary problem

$$\frac{\partial^2\varphi_i}{\partial y^2} + \frac{\partial^2\varphi_i}{\partial z^2} = 0 \quad \text{in } Q_0; \quad \frac{\partial\varphi_i}{\partial n} = 0 \quad \text{on } S_0; \qquad \frac{\partial\varphi_i}{\partial z} = \kappa_i\varphi_i \quad \text{on } \Sigma_0; \quad \int_{\Sigma_0} \varphi_i \mathrm{d}S = 0, \tag{2.5}$$

where the eigenvalues $\kappa_i > 0,\ i \geqslant 1$ determine the natural sloshing frequencies

$$\sigma_i = \sqrt{g\kappa_i}. \tag{2.6}$$

For the circular tank shape, there exist antisymmetric (odd) φ_{2j-1} and symmetric (even) φ_{2i} natural sloshing modes with respect to the Oz-axis. Because the eigenfunctions φ_i are determined by spectral problem (2.5) within a multiplier, a normalization is required. In the present paper, we adopt the following mean square-root normalization:

$$\left.\begin{aligned} &\bar{\varphi}_i(y,z) = \frac{\varphi_i(y,z)}{N_i}, \quad \bar{f}_i = \frac{\varphi_i(y,z_0)}{N_i}, \\ &N_i = \operatorname{sign}(\varphi_i(y_0,z_0))\sqrt{\frac{\displaystyle\int_{-y_0}^{y_0} \varphi_i^2(y,z_0)\,\mathrm{d}y}{y_0}}, \quad y_0 = \sqrt{R_0^2 - z_0^2}. \end{aligned}\right\} \tag{2.7}$$

As long as we know the natural sloshing modes which exactly satisfy the Laplace equation and the zero-Neumann body-boundary condition, the multimodal solution (2.4) exactly satisfies (2.1a) and the body-boundary condition (2.1b). Based on the multimodal solution (2.4), we can then concentrate on kinematic (2.1c) and dynamic (2.1d) boundary conditions to find relationships coupling the generalized coordinates $\beta_i(t)$ and $R_i(t)$. Indeed, substituting the multimodal solution (2.4) into kinematic condition (2.1c) and employing the completeness and orthogonality of $\{\bar{f}_i(y),\ i \geqslant 1\}$ on Σ_0, i.e. $\int_{\Sigma_0} \bar{f}_i\bar{f}_j\,\mathrm{d}S = 0,\ i \neq j$, (Eastham 1962; Lukovsky *et al.* 1984; Morand & Ohayon 1995; Faltinsen & Timokha 2009) gives the relations

$$\dot{\beta}_i = \kappa_i R_i, \ \ i \geqslant 1. \tag{2.8}$$

Furthermore, the orthogonality of $\bar{f}_i$, the dynamic condition (2.1d) and relations (2.8) deduce the following ordinary differential equations:

$$\ddot{\beta}_n + \sigma_n^2\beta_n = K_n(t) = -\frac{\kappa_n\lambda_{2n}}{y_0}\ddot{\eta}_2, \tag{2.9}$$

where the hydrodynamic coefficients λ_{2n}, accounting for the Oz-axis symmetry of $\bar{\varphi}_{2j}$, are defined by

$$\lambda_{2(2j-1)} = \int_{\Sigma_0} y\bar{\varphi}_{2j-1}\,\mathrm{d}y; \quad \lambda_{2(2j)} = \int_{\Sigma_0} y\bar{\varphi}_{2j}\,\mathrm{d}y = 0, \quad j = 1, 2, \ldots. \tag{2.10}$$

The previous derivations show that the original linear sloshing problem (2.1) transforms to an infinite set of uncoupled linear modal equations (2.9) with respect to generalized coordinates $\beta_i(t)$. To describe transient wave elevations by modal solution (2.4*a*), we should numerically integrate modal equations (2.9) with the initial conditions

$$\beta_i(0) = \beta_{0i}, \quad \dot{\beta}_i(0) = \beta_{1i} \tag{2.11}$$

determining the initial free-surface shape and velocity. For the periodic forcing $\eta_j(t) = \eta_{aj}\cos(\sigma t + \sigma_{0j})$, we can analytically find the steady-state surface waves described by the $2\pi/\sigma$-periodic solution of modal equations (2.9):

$$\beta_{2n-1}(t) = \frac{\sigma^2}{\sigma_{2n-1}^2 - \sigma^2}\frac{\kappa_{2n-1}\lambda_{2(2n-1)}}{y_0}\eta_{2a}\cos(\sigma t + \sigma_{02}), \quad \beta_{2n} = 0. \tag{2.12}$$

Because our hydrodynamical model does not account for dissipation, which is small for clean tanks without wave breaking, the absence of damping terms in modal equations (2.9) is an obvious fact. Following Keulegan (1959), we can, however, account for the small viscous energy dissipation due to the boundary layer at the circular and flat endwalls of the horizontal circular tank walls (perpendicular to axis Ox) for a laminar flow and, thereby, modify the linear modal equations. The damping rates ξ_n for each natural mode are

$$\xi_n = \frac{1}{2}\sqrt{\frac{\nu}{2\sigma_n R_0^2}}\left\{\frac{\bar{\gamma}_n}{\kappa_n y_0} + \frac{R_0}{L_1}\right\} = \frac{1}{2}\sqrt{\frac{\nu}{2g^{1/2}R_0^{3/2}}}\left[\kappa_n^{-1/4}\left\{\frac{\bar{\gamma}_n}{\kappa_n y_0} + \frac{R_0}{L_1}\right\}\right], \tag{2.13}$$

where ν is the kinematic viscosity, L_1 is the length of the horizontal circular tank, and the non-dimensional hydrodynamic coefficient $\bar{\gamma}_n$ depends on the tangential velocity at the wetted walls S_0 as follows:

$$\bar{\gamma}_n = \int_{S_0}\left(\frac{\partial\bar{\varphi}_n}{\partial s}\right)^2\mathrm{d}s. \tag{2.14}$$

The damping rates can be incorporated into the linear modal equations (2.9) in the following way:

$$\ddot{\beta}_n + 2\xi_n\sigma_n\dot{\beta}_n + \sigma_n^2\beta_n = K_n(t) = -\frac{\kappa_n\lambda_{2n}}{y_0}\ddot{\eta}_2. \tag{2.15}$$

In summary, derivation of the modal equations (2.9) implicitly assumes that we know the approximate natural sloshing modes φ_i which should exactly satisfy the Laplace equation and the zero-Neumann boundary condition on S_0. Derivation of modal equations (2.9) also uses orthogonality of the natural sloshing modes, and the spectral relation $\partial\varphi_n/\partial z = \kappa_n\varphi_n$ on Σ_0. The latter relation should be accurately approximated in each point of the mean free surface Σ_0. The corresponding approximate natural sloshing modes will be analytically constructed in § 3.

2.3. *Velocity and pressure fields*

Given the natural sloshing modes, the forcing terms associated with η_2 and η_3, and either a steady-state (2.12) or numerical time-integration solution of the modal

equations (2.9) (or (2.15) if we want to account for small damping), we are able to find the absolute velocity field,

$$u = 0, \quad v = \dot{\eta}_2 + \sum_{n=1}^{\infty} \frac{\partial \bar{\varphi}_n}{\partial y} \frac{\dot{\beta}_i}{\kappa_i}, \quad w = \dot{\eta}_3 + \sum_{n=1}^{\infty} \frac{\partial \bar{\varphi}_n}{\partial z} \frac{\dot{\beta}_i}{\kappa_i}. \tag{2.16}$$

The modal expression for the pressure field takes the form

$$p - p_0 = -\rho \left(\frac{\partial \Phi}{\partial t} + gz + gy\eta_4(t) \right) = -\rho \left(y\ddot{\eta}_2 + z\ddot{\eta}_3 + \sum_{i=1}^{\infty} \varphi_i \frac{\ddot{\beta}_i}{\kappa_i} + gz + gy\eta_4(t) \right), \tag{2.17}$$

where ρ is the liquid density and p_0 is the ullage pressure; the g-proportional terms are associated with the hydrostatic pressure component considered in the tank-fixed coordinate system.

2.4. *Resulting hydrodynamic force and moment*

Using general Lukovsky formulas for the hydrodynamic force and moment due to forced liquid sloshing (Lukovsky 1990; Faltinsen & Timokha 2009), or performing direct integration of the pressure (2.17) over the wetted tank surface, we obtain the following modal hydrodynamic force expression for the tank-fixed coordinate system:

$$\left.\begin{aligned} F_2(t) = F_y(t) &= M_l[\{-g\eta_4\} - \ddot{\eta}_2] - \rho L_1 \sum_{j=1}^{\infty} \lambda_{2(2j-1)} \ddot{\beta}_{2j-1}, \\ F_1(t) = F_x(t) &= 0; \quad F_3(t) = F_z(t) = -M_l \ddot{\eta}_3, \end{aligned}\right\} \tag{2.18}$$

where M_l is the liquid mass and L_1 is the tank length along the Ox-axis. The $M_l\{-g\eta_4\}$ term is the liquid weight component in the tank-fixed coordinate system.

The pressure loads on a circular tank cannot cause a hydrodynamic moment around Ox.

2.5. *Non-dimensional hydrodynamic coefficients*

Using the linear modal equations (2.9) or their modification (2.15) is only possible when we know the hydrodynamic coefficients κ_n and λ_n. The computed non-dimensional hydrodynamic coefficients

$$\bar{\kappa}_n = R_0 \kappa_n, \quad \bar{\lambda}_n = R_0^{-2} \lambda_n \quad \text{with } \bar{y}_0 = y_0/R_0, \quad \bar{z}_0 = z_0/R_0, \quad \bar{h} = h/R_0, \tag{2.19}$$

and the damping-rate coefficients $\bar{\gamma}_n$ are listed in tables 1–3 for $0.1 \leqslant h/R_0 \leqslant 1.95$.

3. Analytical approximate natural sloshing modes

In § 3, we assume the geometrical scaling by R_0, so that the non-dimensional spectral problem (2.5) is considered in the circle of radius 1 with the non-dimensional liquid depth $\bar{h} = h/R_0$ varying between 0 and 2; other non-dimensional parameters are defined by (2.19).

The Trefftz solution of this non-dimensional spectral problem will be constructed by using analytically given trial functions which exactly satisfy the Laplace equation and the zero-Neumann boundary condition on S_0. To find these trial functions, we conformally transform the whole interior tank domain, including the 'air-occupied' domain, to a half-plane so that the tank surface, except the upper circle pole, becomes the horizontal axis (see figure 2).

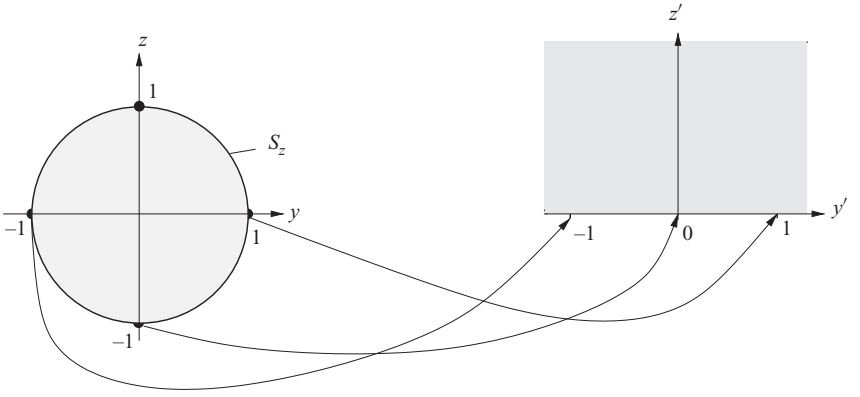

FIGURE 2. Conformal transformation of the whole tank domain defined by (3.1*a*). S_z is the circle without upper pole (0, 1) providing $S_0 \subset S_z$ for any $0 < \bar{h} < 2$.

3.1. *Two families of trial functions*

The conformal transformation in figure 2 can be defined by the formulas

$$y' = \frac{2y}{y^2 + (z-1)^2}, \quad z' = -1 - \frac{2(z-1)}{y^2 + (z-1)^2}, \tag{3.1a}$$

$$y = \frac{2y'}{y'^2 + (z'+1)^2}, \quad z = 1 - \frac{2(z'+1)}{y'^2 + (z'+1)^2} \tag{3.1b}$$

in the Cartesian coordinates Oyz and $O'y'z'$, respectively. When applied to the mean liquid domain Q_0, this transformation (see figure 3) maps segment Q_0 to another segment Q_0' so that the arc S_0 becomes the chord S_0' lying on the horizontal axis Oy', and the chord Σ_0 transforms to the arc Σ_0', i.e.

$$Q_0 = \{y^2 + z^2 < 1,\ z < \bar{z}_0\} \ \rightarrow\ Q_0' = \{y'^2 + (z' - z_0')^2 < R_0'^2,\ z' > 0\}, \tag{3.2}$$

where

$$\left.\begin{aligned} &\bar{z}_0 = \bar{h} - 1, \quad z_0' = \frac{\bar{z}_0}{1 - \bar{z}_0}, \quad \bar{y}_0 = \sqrt{1 - \bar{z}_0^2}, \\ &y_0' = \sqrt{\frac{1 + \bar{z}_0}{1 - \bar{z}_0}} = R_0' \sqrt{1 - \bar{z}_0^2}, \quad \theta_0 = \arccos(\bar{z}_0), \end{aligned}\right\} \tag{3.3}$$

$$\left.\begin{aligned} &R_0' = 1 + z_0' = \frac{1}{1 - \bar{z}_0}, \quad w_3 = (-\bar{y}_0, \bar{z}_0), \\ &w_4 = (\bar{y}_0, \bar{z}_0), \quad w_3' = (-y_0', 0), \quad w_4' = (y_0', 0). \end{aligned}\right\} \tag{3.4}$$

The radius of the arc S_0 is equal to 1, and the radius R_0' of Σ_0' monotonically increases from 1/2 to infinity as $\bar{z}_0$ (the vertical position of the mean free surface Σ_0) varies from -1 to 1.

According to substitution (3.1*b*), the natural sloshing modes (eigenfunctions $\varphi_n(y, z)$) transform to

$$\varphi_n'(y', z') = \varphi_n \left(\frac{2y'}{y'^2 + (z'+1)^2}, 1 - \frac{2(z'+1)}{y'^2 + (z'+1)^2} \right), \tag{3.5}$$

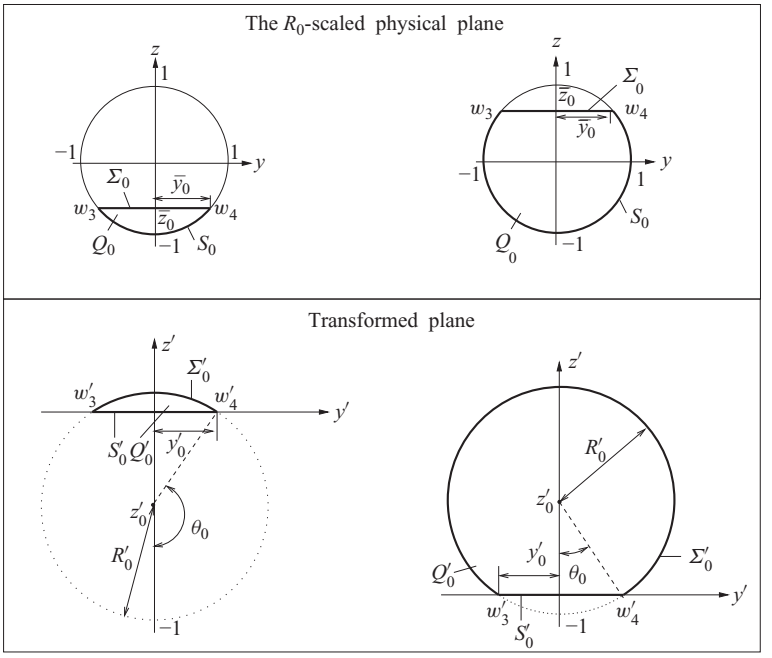

FIGURE 3. The mean liquid domain Q_0 in the R_0-scaled physical plane for $\bar{h} = h/R_0 < 1$ and $\bar{h} > 1$, and the corresponding transformed domains Q_0' defined by (3.1a) in the transformed plane.

which are solutions of the following spectral problem:

$$\left.\begin{aligned} &\nabla^2\varphi_n' = 0 \quad \text{in } Q_0', \qquad \frac{\partial\varphi_n'}{\partial z'} = 0 \quad \text{on } S_0', \\ &\frac{\partial\varphi_n'}{\partial n} = \frac{\bar{\kappa}_n(1-\bar{z}_0)}{1+z'}\varphi_n' \quad \text{on } \Sigma_0', \quad \int_{\Sigma_0'} \frac{\varphi_n'\,\mathrm{d}S}{y'^2+(z'+1)^2} = 0 \end{aligned}\right\} \tag{3.6}$$

in the $O'y'z'$-plane. In turn, if φ_n' is an eigenfunction of the problem (3.6),

$$\varphi_n(y,z) = \varphi_n'\left(\frac{2y}{y^2+(z-1)^2}, -1-\frac{2(z-1)}{y^2+(z-1)^2}\right) \tag{3.7}$$

is the corresponding eigenfunction of the spectral boundary problem (2.5).

The 'first family' of trial functions in the transformed plane consists of the z'-even harmonic polynomials (polynomials satisfying the Laplace equation as well as the zero-Neumann condition at $z' = 0$) which are, for example, defined by Vekua (1953, 1967) and Lukovsky *et al.* (1984):

$$W_i'(y',z') = \sum_{k=0}^{[i/2]} (-1)^k C_i^{2k} y'^{i-2k} z'^{2k}, \quad i = 0, 1, \ldots. \tag{3.8}$$

Here, $[i/2]$ is the integer part of $i/2$, and $C_i^{(2k)} = (2k)!/(i\,!(2k-i)!)$.

Explicit expressions for the harmonic polynomials are

$$W_0' = 1, \quad W_1' = y', \quad W_2' = y'^2 - z'^2, \quad W_3' = y'^3 - 3y'z'^2, \ldots. \tag{3.9}$$

Substitution of the variables y' and z' (3.1a) into the functions $W_i'(y', z')$ yields the trial functions $W_i(y, z)$ in the physical plane satisfying both the Laplace equation and the zero-Neumann condition on S_0:

$$W_0(y,z)=1, \quad W_1(y,z)=\frac{2y}{y^2+(z-1)^2}, \quad W_2(y,z)=\frac{2y^2+(y^2+z^2+1)^2}{(y^2+(z-1)^2)^2}, \ \ldots. \tag{3.10}$$

The uniform horizontal steady flow in the transformed plane (corresponding to $W_1' = y'$) is the same as the horizontal dipole-type solution $W_1(y, z)$, with singularity at the 'upper pole' in the physical plane. The latter solution with depth-dependent singularity position has been extensively discussed by Faltinsen & Timokha (2009) as giving a satisfactory approximation of the first natural sloshing mode.

The second trial function, $W_2(y, z)$, is a linear combination of the vertical dipole-type solution, $V_1(y, z)$, $\partial W_1/\partial y$, and a constant, i.e.

$$W_2(y,z)=2\frac{\partial W_1}{\partial y}-2V_1-1. \tag{3.11}$$

Because the harmonic polynomials $W_i'(y'z')$ are infinitely differentiable functions in the whole transformed plane $O'y'z'$, the harmonic functions $W_i(x, y)$ are also infinitely differentiable functions in the physical plane except the upper circle pole $(0, 1)$. However, this contradicts the theorems of Komarenko (1980):

At the corner points between Σ_0 and S_0 of the R_0-scaled two-dimensional spectral boundary problem (2.5), the asymptotic behaviour of the natural sloshing modes (eigenfunctions) φ_n is described by real and imaginary parts of $\mathscr{Z}^{\alpha k}$ and $\mathscr{Z}^p \ln^q \mathscr{Z}$ ($\mathscr{Z} = (y \pm \bar{y}_0) + \mathrm{i}(z - \bar{z}_0)$), where $\alpha = \pi/\theta_i$ and θ_i is the inner angle between Σ_0 and S_0, and k, p and q are nonnegative integers. Appearance of the corresponding asymptotic terms depends on the real number α, i.e. (i) when α is an irrational number, there are only the $\mathscr{Z}^{\alpha k}$-type quantities in the local asymptotic solution, (ii) when $\alpha = m$ is an integer number, the $\mathscr{Z}^{\alpha k}$-type components become the polynomials, but there appear the log-type quantities $\mathscr{Z}^{m(k+i)} \ln^{1+i} \mathscr{Z}$, $i = 0, 1, \ldots$; $k = 1, 2, \ldots$, and, finally, (iii) when $\alpha = m/n$ is the rational number (m/n is the irreducible fraction), both $\mathscr{Z}^{\alpha k}$ and $\mathscr{Z}^{m(k+i)} \ln^{1+i} \mathscr{Z}$, $i = 0, 1, \ldots$; $k = 1, 2, \ldots$ asymptotic terms are possible.

The readers can also see related mathematical results for the mixed boundary condition by Wigley (1964). The eigenfunctions of the two-dimensional spectral boundary problem (2.5) are characterized by singular asymptotic behaviour, so that the higher-order derivatives of φ_n become infinite at the corner points formed by S_0 and Σ_0.

The singular asymptotic corner-points behaviour of the natural sloshing modes should, generally, be accounted for by trial functions in the Trefftz solution. This is especially important for $\bar{h} \geqslant 1$ when the singularity appears in the second-order derivatives. Indeed, considering lower liquid depths, $0 < \bar{h} < 1$ with $2 < \alpha = \pi/\theta_i$ (θ_i is the inner angle between Σ_0 and S_0) detects continuous second-order derivatives at the corner points. However, higher liquid depths, $1 \leqslant \bar{h} < 2$, lead to $1 < \alpha \leqslant 2$ and, therefore, the second-order derivatives become infinite at the corner points. The most singular $\mathscr{Z} \ln \mathscr{Z}$-type asymptotics (infinite first-order derivatives, $\mathscr{Z} = (y \pm \bar{y}_0) + \mathrm{i}(z - \bar{z}_0)$) is expected as $\bar{z}_0 \to 1$ ($\bar{h} \to 2$). This limit caused by $\alpha \to 1$ leads to the so-called ice-fishing problem in the non-scaled physical plane, by letting Σ_0 be finite with increasing $R_0 \to \infty$. Another interesting case is $\theta_i = (1/2)\pi$ (semicircle) associated with $\alpha = 2$. We should then expect the log-type $\mathscr{Z}^2 \ln \mathscr{Z}$-asymptotics at the corner points.

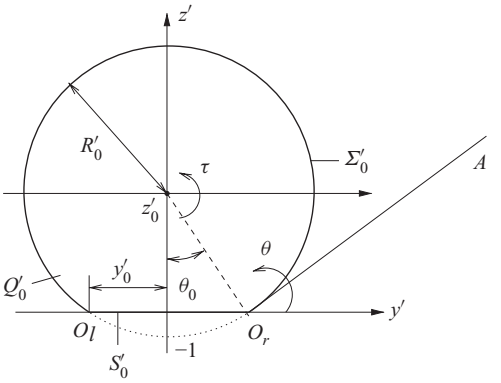

FIGURE 4. Sketch of the transformed domain with notations needed to construct trial functions capturing the corner-point asymptotics. The inner angle between $O_l O_r$ and $O_r A$ is equal to $\theta_i = \pi - \theta_0$.

Remembering that the used conformal transformation (3.1) keeps the same inner angle between S_0 and Σ_0, and S_0' and Σ_0', respectively, we start working in the transformed plane (figure 4) to construct a 'second family' of trial harmonic functions. These harmonic functions should satisfy the zero-Neumann condition on $(O_r O_l)$ and capture the required corner-point asymptotics. For brevity, we assume that $\alpha = \pi/\theta_i$ is an irrational number and, furthermore, concentrate on a spectral boundary condition on Σ_0' (in (3.6)) in the vicinity of O_r. After introducing the local polar coordinate system $r = \sqrt{(y' - y_0')^2 + z'^2}$, $\theta = \arccos(y'/r)$, this boundary condition takes the form

$$\frac{\partial \varphi'}{\partial r}\cos(\tau - \theta) + \frac{1}{r}\frac{\partial \varphi'}{\partial \theta}\sin(\tau - \theta) = \frac{\kappa}{R_0'(1 + z')}\varphi', \tag{3.12}$$

where the angle τ is shown in figure 4. Furthermore, a local harmonic solution at O_r can be postulated as

$$r^{\alpha_i}\cos(\alpha_i(\theta - \pi)), \quad i = 1, \ldots \tag{3.13}$$

to satisfy the zero-Neumann boundary condition on (O_l, O_r). Substituting expression (3.13) into the boundary condition (3.12) and noting that $\tau - \theta = -(1/2)\pi + O(r)$ and $\partial\varphi'/\partial r \sim r^{-1}\partial\varphi'/\partial\theta$ as $r \to 0$, one can extract the primary asymptotic terms of (3.12):

$$-\frac{\partial \varphi'}{\partial \theta} + O(r^{\alpha+1}) = \frac{r\kappa}{R_0'(1 + z')}\varphi' \quad \text{on } (O_l A). \tag{3.14}$$

The latter asymptotic boundary condition means that (3.12) is in the lowest-order approximation equivalent to the Neumann boundary condition $\partial\varphi'/\partial\theta = 0$ for $\theta = \theta_0$ and, therefore,

$$\alpha_i = \frac{\pi i}{\theta_i} = \alpha i, \quad i = 1, 2, \ldots \tag{3.15}$$

in the local harmonic solution (3.13). This result is consistent with Komarenko's theorem.

Considering the local harmonic solution (3.13) in the $Oy'z'$-coordinates, we arrive at the following expressions:

$$\phi'_{IIi} = r^{\alpha_i}\cos\left(\alpha_i\left(\pi - \arccos\frac{y'-y'_0}{r}\right)\right) = ((y'-y'_0)^2 + z'^2)^{(1/2)\alpha_i} \times \cos\left(\alpha_i\left(\pi - \arccos\frac{y'-y'_0}{\sqrt{(y'-y'_0)^2+z'^2}}\right)\right). \quad (3.16)$$

Analogously, one can get the local harmonic solution at O_l:

$$\phi'_{Ii} = ((y'+y'_0)^2 + z'^2)^{(1/2)\alpha_i}\cos\left(\alpha_i\ \arccos\frac{y'+y'_0}{\sqrt{(y'+y'_0)^2+z'^2}}\right). \quad (3.17)$$

Finally, combining (3.16) and (3.17), we can get the stated second family of singular harmonic antisymmetric and symmetric (with respect to the Oy'-axis) trial functions as follows:

$$\phi'_{2i-1}(y',z') = \phi'_{Ii} - \phi'_{IIi};\quad \phi'_{2i-2}(y',z') = \phi'_{Ii} + \phi'_{IIi},\ i = 1,2,\ldots. \quad (3.18)$$

Obviously, these harmonic functions and their harmonic originals (due to substitution (3.1a)) in the physical plane satisfy the zero-Neumann condition on S'_0 and S_0, respectively.

The trial functions (3.16)–(3.18) completely account for the corner-point asymptotics only for the irrational numbers $\alpha_i = \alpha i$. When α is an irreducible fraction m/n, there exists an integer subsequence $\{\alpha_{i_j} = \alpha_{n(j+1)} = m(j+1),\ j = 0,1,\ldots\}$ providing, in accordance with Komarenko's theorem, the log-type asymptotic terms at the corner points. Let us assume that α remains an irrational number, but the subsequent numbers $\alpha_{i_j} = \alpha i_j$ include elements which are close to $m = 1,2,\ldots$, i.e.

$$\alpha i_j - m(1+j) = (1+j)O(\delta),\quad j = 0,1,\ldots,\quad \text{where } |\delta| \ll 1. \quad (3.19)$$

Combining the complex functions $\mathscr{Z}^{\alpha n_j}$ and $\mathscr{Z}^{m(1+j)}$ (here, $\mathscr{Z} = (y' \pm y'_0) + \mathrm{i}z'$ in the complex transformed plane) via

$$\boxed{\mathscr{Z}^m\frac{\mathscr{Z}^{O(\delta)}-1}{O(\delta)}}, \ldots, \mathscr{Z}^{m(k+1)}\frac{\mathscr{Z}^{O(\delta)}-1}{O(\delta)}, \ldots, \quad (3.20a)$$

$$\ldots,\ldots,\ldots,\ldots,\ldots,\ldots,\ldots,\ldots,\ldots,\ldots,\ldots,$$

$$\mathscr{Z}^{m(j+1)}\left(\frac{\mathscr{Z}^{O(\delta)}-1}{O(\delta)}\right)^{1+j}, \ldots, \mathscr{Z}^{m(j+k)}\left(\frac{\mathscr{Z}^{O(\delta)}-1}{O(\delta)}\right)^{1+j}, \ldots \quad (3.20b)$$

leads to the theoretically expected log-type terms at O_r as $\delta \to 0$. This means that the log-type asymptotics in Komarenko's results on the natural sloshing modes is a consequence of combined terms involving the local harmonic solutions such as (3.13) and the corresponding harmonic polynomials when the irrational number α is close to a rational number.

To handle the log-type asymptotics with trial functions (3.18), we can also use combinations of the harmonic polynomials and trial functions (3.18). In calculations, we should assume that α always remains an irrational number (within a small correcting number comparable with an admissible calculation error, if needed) and combine $W'_i(y' \pm y'_0, z')$ and $\phi'_i(y',z')$ similarly to expressions (3.20).

The lowest-order log-type asymptotics (framed box in (3.20a)) is associated with the $\mathscr{Z}^m(\mathscr{Z}^{O(\delta)}-1)/O(\delta)$ term. Whereas α is close to the irreducible fraction m/n,

remembering that $\phi'_n(y', z')$ corresponds to the $\mathscr{Z}^{\alpha n}$-type asymptotic terms at the corner points and W'_m is the m-order polynomials, this log-type asymptotics can be captured by modifying the trial function $\phi'_n(y', z')$ as follows:

$$\phi'_n(x', z') := \frac{\phi'_n(x', z') - [W'_m(y' + y'_0, z') + (-1)^n W'_m(y' - y'_0, z')]}{\alpha n - m} \tag{3.21}$$

(the term $(-1)^n$ is introduced to get antisymmetric and symmetric trial functions for odd and even n, respectively). Combining expressions for the higher-order log-type asymptotics from (3.20) leads to more complicated expressions which, as we found out in numerical experiments, may matter only in the limit case $\bar{h} \to 2$.

3.2. *The Trefftz solution*

The Trefftz variational method in the transformed plane assumes the eigenfunctions of the spectral boundary problem (3.6) to be

$$\varphi'(y', z') = \sum_{i=0}^{q} c_i \Phi'_i(y', z'), \tag{3.22}$$

where $\{\Phi'_i\}$ is a set of trial harmonic functions satisfying the zero-Neumann boundary condition on S'_0, and the c_i are the unknown weight coefficients. Mathematically, the traces $\Phi'|_{\Sigma'_0}$ should constitute a complete set of functions in the mean square-root metrics on Σ'_0.

After substituting variables (3.1*a*), solution (3.22) becomes defined in the physical plane, i.e.

$$\varphi(y, z) = \sum_{i=0}^{q} c_i \Phi_i(y, z), \tag{3.23}$$

where the trial harmonic functions $\Phi_i(y, z)$ satisfy the zero-Neumann condition on S_0. To find the Trefftz solution φ of the spectral boundary problem (2.5), we can use the variational equality following from minimizing the Rayleigh quotient (see Morand & Ohayon 1995; Faltinsen & Timokha 2009),

$$\int_{\Sigma_0} \delta\varphi \left(\frac{\partial \varphi}{\partial z} - \bar{\kappa}\varphi \right) \mathrm{d}S = 0, \tag{3.24}$$

with $\delta\varphi = \Phi_i$, $i = 0, \ldots, q$. This variational equality leads to the spectral matrix problem

$$(A - \bar{\kappa} B)\boldsymbol{c} = 0, \quad \boldsymbol{c} = (c_0, \ldots, c_q), \tag{3.25}$$

where A and B are symmetric matrices with elements

$$\left.\begin{aligned} a_{ij} &= R'_0 \int_{-\pi/2+\theta_0}^{3\pi/2-\theta_0} \left[\Phi'_i \frac{\partial \Phi'_j}{\partial n'} \right]_{\substack{y'=R'_0\cos\tau \\ z'=R'_0\sin\tau}} \mathrm{d}\tau, \\ b_{ij} &= \frac{1}{R'_0} \int_{-\pi/2+\theta_0}^{3\pi/2-\theta_0} \left[\frac{\Phi'_i \Phi'_j}{1+\sin\tau} \right]_{\substack{y'=R'_0\cos\tau \\ z'=R'_0\sin\tau}} \mathrm{d}\tau. \end{aligned}\right\} \tag{3.26}$$

Here, n' is the outer normal to Σ'_0, R'_0 is the radius of Σ'_0 and the angle τ is defined in figure 4.

The eigenvalues $\bar{\kappa}$ of the spectral matrix problem (3.25) approximate the eigenvalues of the original spectral boundary problem. Substituting the orthogonal eigenvectors $(c_0, \ldots, c_q)$ into representation (3.23) also gives the corresponding approximate natural

$\bar{h}$	$\bar{\kappa}_1$	$\bar{\kappa}_2$	$\bar{\kappa}_3$	$\bar{\kappa}_4$	$\bar{\kappa}_5$	$\bar{\kappa}_6$	$\bar{\kappa}_7$	$\bar{\kappa}_8$	$\bar{\kappa}_9$
0.1	1.02092	2.96076	5.64616	8.86373	12.4067	16.1099	19.8655	23.6177	27.3459
0.2	1.04385	2.92908	5.35498	8.03025	10.7672	13.4884	16.1797	18.8477	21.5002
0.3	1.06908	2.90549	5.12073	7.42633	9.71129	11.9646	14.1976	16.4190	18.6338
0.4	1.09698	2.89054	4.93704	6.99058	9.00749	11.0013	12.9835	14.9595	16.9320
0.5	1.12800	2.88487	4.79798	6.67865	8.52709	10.3602	12.1862	14.0084	15.8285
0.6	1.16268	2.88924	4.69867	6.46064	8.19875	9.92609	11.6490	13.3690	15.0877
0.7	1.20173	2.90466	4.63560	6.31715	7.98200	9.63874	11.2925	12.9440	14.5945
0.8	1.24606	2.93246	4.60670	6.23613	7.85373	9.46499	11.0741	12.6812	14.2877
0.9	1.29685	2.97444	4.61145	6.21093	7.80143	9.38696	10.9706	12.5528	14.1343
1.0	1.35573	3.03310	4.65105	6.23920	7.81986	9.39668	10.9718	12.5457	14.1189
1.1	1.42489	3.11203	4.72882	6.32264	7.90985	9.49400	11.0765	12.6580	14.2389
1.2	1.50751	3.21640	4.85091	6.46747	8.07834	9.68639	11.2932	12.8988	14.5041
1.3	1.60830	3.35408	5.02774	6.68598	8.34014	9.99089	11.6412	13.2899	14.9388
1.4	1.73463	3.53751	5.27678	6.99993	8.72206	10.4388	12.1571	13.8722	15.5888
1.5	1.89888	3.78768	5.62838	7.44799	9.27201	11.0868	12.9063	14.7200	16.5377
1.6	2.12372	4.14328	6.13932	8.10314	10.0807	12.0419	14.0138	15.9749	17.9442
1.7	2.45669	4.68569	6.92979	9.12053	11.3415	13.5329	15.7458	17.9389	20.1479
1.8	3.02140	5.62694	8.31385	10.9061	13.5596	16.1586	18.7997	21.4033	24.0381
1.9	4.31118	7.81443	11.5484	15.0852	18.7600	22.3180	25.9691	29.5463	33.1772
1.95	6.15096	10.9625	16.2141	21.1172	26.2727	31.2168	36.3324	41.3124	46.3937

TABLE 1. Non-dimensional eigenvalues $\bar{\kappa}_i = \kappa_i R_0,\ i = 1, \ldots, 9$ versus non-dimensional liquid depth $\bar{h} = h/R_0$.

sloshing modes which constitute, due to orthogonality of the eigenvectors $(c_0, \ldots, c_q)$, the *orthogonal traces* $\varphi_i|_{\Sigma_0} = f_i(y)$ on Σ_0 for the Trefftz eigensolutions (3.23) as discussed in § 2.2.

When employing the two families of constructed trial functions in the Trefftz solution (3.22), we distinguish antisymmetric and symmetric natural modes, i.e.

$$\left.\begin{aligned} \varphi'_{2k-1} &= \sum_{i=1}^{q_1} c_i W'_{2i-1} + \sum_{i=1}^{q_2} c_{q_1+i}\phi'_{2i-1} = \sum_{j=1}^{q_1+q_2} c_j \Phi'_j, \quad k = 1, 2, \ldots, \\ \varphi'_{2k} &= \sum_{i=0}^{q_1} c_i W'_{2i} + \sum_{i=0}^{q_2} c_{q_1+i+1}\phi'_{2i} = \sum_{j=0}^{q_1+q_2+1} c_j \Phi'_j, \quad k = 0, 1, \ldots, \end{aligned}\right\} \tag{3.27}$$

where the first sums (up to q_1) in expressions for φ'_{2k-1} and φ'_{2k} include the harmonic polynomials, but the second sums are based on the singular trial functions capturing the corner-point asymptotics.

The numerical hydrodynamic coefficients computed by using the approximate natural sloshing modes (3.27) with normalization (2.7) are listed in tables 1–3.

Details on convergence and error of the Trefftz solution (3.27) for the non-dimensional eigenvalues $\bar{\kappa}_i$ and the natural sloshing modes φ_i are reported in the supplementary material available at journals.cambridge.org/flm. It is important that the present Trefftz solution provides a uniform convergence to the spectral boundary condition of (2.5) on Σ_0. For middle and higher liquid depths, $1.0 \leqslant h/R_0$, this convergence is only possible due to the singular trial functions. The consequence of the singularity at the intersection between the mean free surface and the tank wall is infinite second- and higher-order derivatives of the free-surface profile, and the associated velocity potential, at the intersection point. However, the free-surface elevation and the velocity field remain finite at this intersection point. The wave slope

$\bar{h}$	$\bar{\lambda}_{21}$	$\bar{\lambda}_{23}$	$\bar{\lambda}_{25}$	$\bar{\lambda}_{27}$	$\bar{\lambda}_{29}$
0.1	0.155126	0.001617	0.000127	0.000024	0.000007
0.2	0.293875	0.006068	0.000864	0.000256	0.000107
0.3	0.416210	0.012741	0.002468	0.000896	0.000430
0.4	0.522105	0.021049	0.004950	0.002014	0.001041
0.5	0.611544	0.030452	0.008188	0.003586	0.001947
0.6	0.684522	0.040456	0.011994	0.005534	0.003116
0.7	0.741044	0.050598	0.016152	0.007756	0.004492
0.8	0.781124	0.060439	0.020443	0.010132	0.006003
0.9	0.804786	0.069554	0.024644	0.012538	0.007569
1.0	0.812062	0.077529	0.028538	0.014844	0.009107
1.1	0.802998	0.083954	0.031912	0.016919	0.010526
1.2	0.777645	0.088423	0.034552	0.018629	0.011734
1.3	0.736069	0.090528	0.036245	0.019838	0.012635
1.4	0.678346	0.089857	0.036771	0.020403	0.013128
1.5	0.604565	0.085985	0.035903	0.020176	0.013105
1.6	0.514833	0.078467	0.033394	0.018993	0.012447
1.7	0.409283	0.066817	0.028974	0.016672	0.011023
1.8	0.288084	0.050477	0.022312	0.012993	0.008667
1.9	0.151479	0.028703	0.012964	0.007651	0.005152
1.95	0.077529	0.015411	0.007055	0.004198	0.002842

TABLE 2. Five lowest non-zero non-dimensional hydrodynamic coefficients $\bar{\lambda}_{2i} = \lambda_{2i}/R_0^2$ versus $\bar{h} = h/R_0$.

$\bar{h}$	$\bar{\gamma}_1$	$\bar{\gamma}_2$	$\bar{\gamma}_3$	$\bar{\gamma}_4$	$\bar{\gamma}_5$	$\bar{\gamma}_6$	$\bar{\gamma}_7$	$\bar{\gamma}_8$	$\bar{\gamma}_9$
0.1	6.444	29.30	71.08	126.4	187.2	246.6	302.1	353.9	403.5
0.2	4.379	18.23	38.67	59.85	78.83	96.01	112.5	129.0	145.5
0.3	3.437	13.09	24.82	35.13	44.18	52.95	61.77	70.68	79.66
0.4	2.864	10.01	17.31	23.31	28.94	34.61	40.36	46.16	51.98
0.5	2.467	7.935	12.78	16.82	20.85	24.94	29.08	33.24	37.41
0.6	2.171	6.455	9.859	12.89	15.99	19.14	22.31	25.50	28.68
0.7	1.941	5.357	7.888	10.33	12.82	15.36	17.89	20.45	22.99
0.8	1.757	4.520	6.508	8.566	10.63	12.74	14.84	16.96	19.06
0.9	1.607	3.871	5.515	7.295	9.054	10.86	12.64	14.45	16.24
1.0	1.484	3.361	4.786	6.346	7.888	9.454	11.02	12.58	14.18
1.1	1.383	2.959	4.242	5.632	7.010	8.405	9.795	11.20	12.58
1.2	1.302	2.640	3.837	5.081	6.348	7.602	8.870	10.15	11.40
1.3	1.239	2.390	3.540	4.662	5.855	7.007	8.179	9.403	10.51
1.4	1.194	2.199	3.332	4.354	5.504	6.583	7.684	8.899	9.868
1.5	1.171	2.061	3.208	4.149	5.288	6.330	7.376	8.649	9.468
1.6	1.175	1.977	3.172	4.011	5.214	6.067	7.267	8.128	9.322
1.7	1.222	1.963	3.256	4.033	5.329	6.124	7.412	8.221	9.500
1.8	1.353	2.065	3.557	4.298	5.793	6.558	8.041	8.817	10.29
1.9	1.739	2.487	4.493	5.234	7.284	8.015	10.08	10.77	12.85
1.95	2.351	3.218	5.989	6.807	9.644	10.49	13.36	14.20	17.12

TABLE 3. Non-dimensional hydrodynamic coefficients $\bar{\gamma}_i$ defined by (2.14) and involved in computation of the linear damping ratios (2.13) versus non-dimensional liquid depth $\bar{h} = h/R_0$.

is also finite except in the limit $h/R_0 \to 2$, which corresponds to the 'ice-fishing' problem. In practice, the local wave steepness at the intersection point increases with h/R_0, indicating increased importance of nonlinearities. The fact that the second

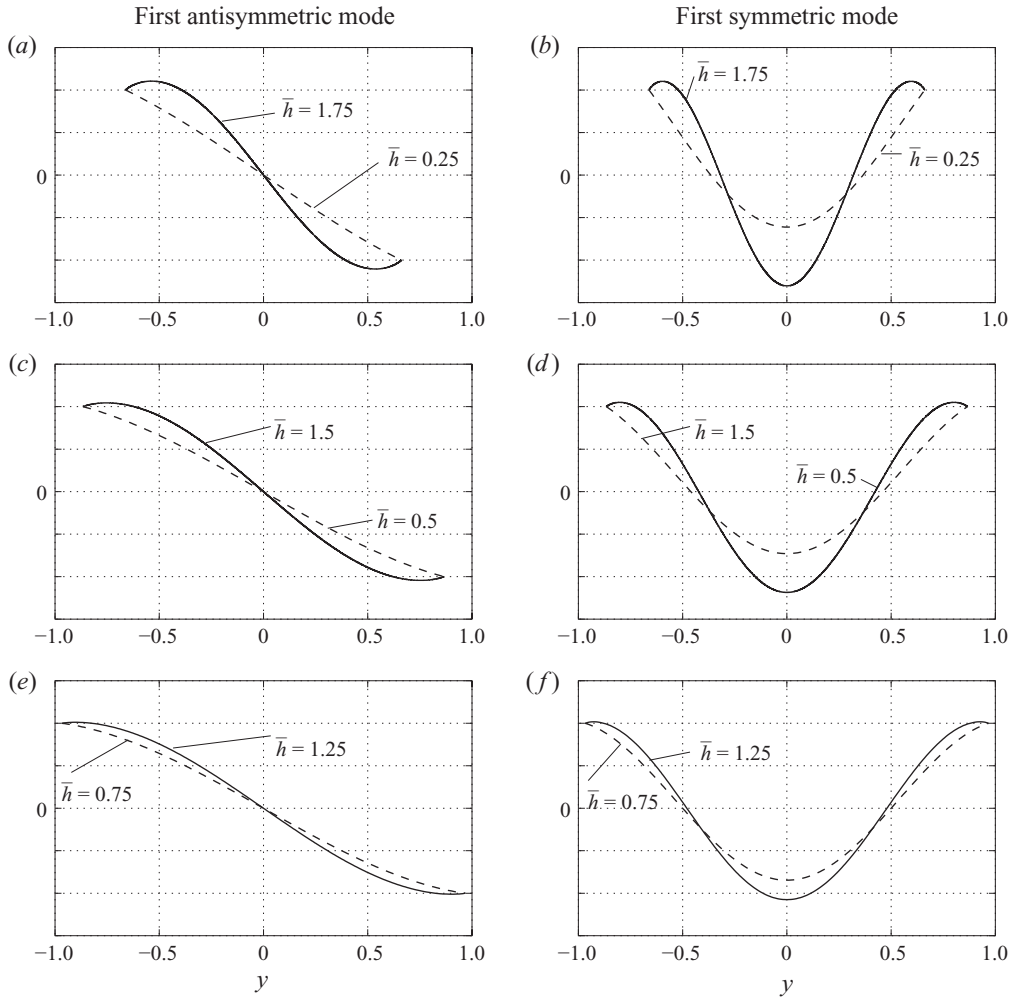

FIGURE 5. Surface-wave profiles associated with lower natural sloshing modes. The vertical wave elevations are normalized to provide the same value at $y = -\bar{y}_0$. The first antisymmetric mode and the first symmetric mode correspond to $\bar{\kappa}_1$ and $\bar{\kappa}_2$, respectively.

derivative of the wave elevation is infinite at the intersection points implies that surface tension may matter.

The predicted two lowest natural modes will be compared with the 'high-spot' results by Kulczycki & Kuznetsov (2009) which state that, if the tank walls are not vertical and the inner angle between Σ_0 and S_0 exceeds $(1/2)\pi$, the maximum wave elevation is expected away from the wall. The inner angles exceeding $(1/2)\pi$ appear in the studied case for $\bar{h} > 1$. A basis for Kulczycki & Kuznetsov's (2009) analysis is the previously described singular flow behaviour at the intersection between the mean free surface and the tank wall. Our numerical method provides uniform convergence to the natural modes and, therefore, is able to illustrate the surface-wave profiles as well as the trend in changing local wave steepness with increasing tank filling. Results on the surface profiles of the two lowest natural modes are shown in figure 5 for non-dimensional depths $\bar{h} = h/R_0 = 0.25, 0.5, 0.75, 1.25, 1.5$ and 1.75.

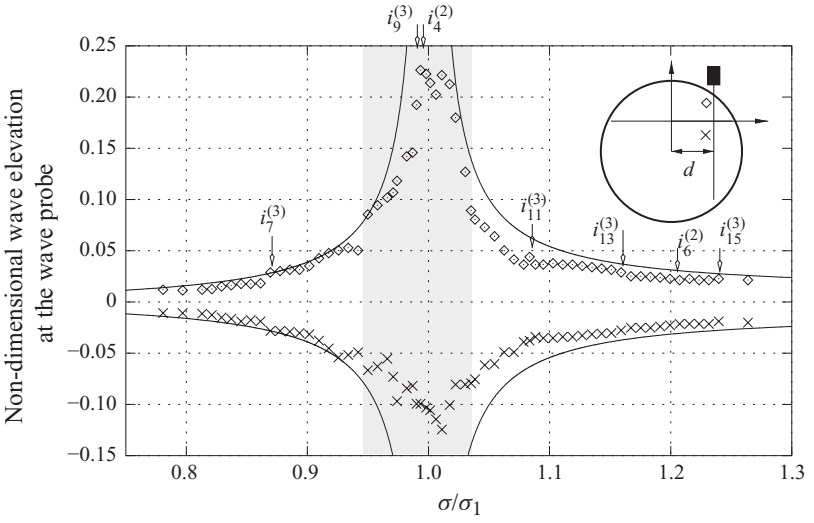

FIGURE 6. The steady-state (maximum and minimum) wave elevation at the wave probe situated at $d = 0.603777R_0$. Comparison between experimental data by Bogomaz & Sirota (2002) and the linear multimodal theory (4.1). The wave elevations are normalized by $R_0 = 0.1325$ m. The longitudinal tank dimension of the Lucite tank is $L_1 = 0.95$ m, the horizontal forcing amplitude is $\eta_{2a} = 0.0075472R_0$. The tank filling is $h/R_0 = 1.47$. The shadow zone notes the frequency range, where Bogomaz & Sirota (2002) report on strongly nonlinear three-dimensional waves due to amplification of longitudinal modes. The possibility of the secondary resonance due to the second- and third-order nonlinearities is indicated by $i_k^{(i)}$, where k is the number of the corresponding mode and i is the order of nonlinearity.

For small liquid depths, the first antisymmetric mode is of a clearly linear character, e.g. $\varphi_1(y, \bar{z}_0) = f_i(y) \approx Cy$, where C is a constant. As we report in the supplementary material, the lowest natural sloshing mode φ_1 is dominantly contributed by the horizontal dipole-type flow with the singularity at the upper circle pole. In the limit shallow liquid case ($\bar{h} \to 0$), this dipole-type flow causes the liquid motions along the circular wall to behave as a 'frozen' liquid mass, which implies $\bar{\kappa}_1 = 1$ by using a pendulum model. Indeed, according to table 1, the eigenvalues $\bar{\kappa}_1$ become close to 1 for smaller liquid depths. The second (first symmetric) natural mode also implies non-steep surface-wave profiles for lower liquid depths.

4. Comparison with experiments and nonlinear computational-fluid-dynamics simulations

4.1. *Steady-state vertical free-surface wave elevation*

The fact that the theory predicts a non-zero value of the free-surface elevation at the intersection point does not make sense for $h/R_0 \neq 1$ due to conflict with the tank wall geometry. Our focus is, therefore, on the wave elevation slightly away from circular walls, as shown for an experimental case in figure 6.

Experimental steady-state wave elevations (maximum and minimum) with the input parameters given in the caption of figure 6 were presented by Bogomaz & Sirota (2002) for a wide range of forcing frequencies. The non-dimensional depth is $h/R_0 = 1.47$ and the forcing amplitude η_{2a} is small and equal to $0.0076R_0$. Employing representation (2.4*a*) and steady-state solution (2.12) for sway excitations, we arrive

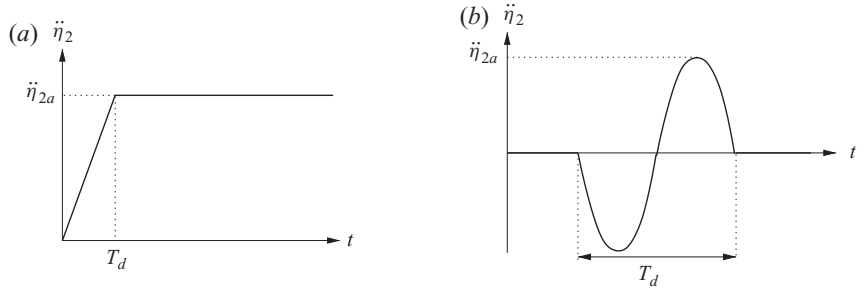

FIGURE 7. Transverse acceleration of the tank associated with (*a*) the turning manoeuvre and (*b*) the lane change of a tanker vehicle.

at the following expression for the steady-state elevation amplitude at $y = d$:

$$\frac{R_0\sigma^2}{y_0}\sum_{i=1}^{\infty}\frac{\bar{\kappa}_{2i-1}\bar{\lambda}_{2(2i-1)}}{\sigma_{2i-1}^2-\sigma^2}\eta_{2a}\bar{f}_{2i-1}(d). \tag{4.1}$$

Linear multimodal prediction (4.1) is compared with these experimental measurements in figure 6. The shadow zone denotes the frequency range, where Bogomaz & Sirota (2002) reported a transition to strongly three-dimensional waves. A linear sloshing theory cannot predict such a transfer of energy to three-dimensional wave motions. Away from this zone, the theoretical predictions are in satisfactory agreement with experiments.

The literature also contains experiments by Kobayashi *et al.* (1989) and Navarrete *et al.* (2003) on the steady-state hydrodynamic force conducted with larger forcing amplitudes, $0.01R_0 \lesssim \eta_{2a}$, in a wide frequency range around σ_1. Our attempts to compare with these experimental data close to and away from σ_1 were not successful. The linear multimodal solution gives much larger values of the hydrodynamic force than the measurements. This fact, and the photograph in the original figure 18 by Kobayashi *et al.* (1989) showing an overturning of the free surface at the wall, indicates limitations of linear sloshing theory in steady-state nearly resonant conditions.

4.2. *Transient horizontal hydrodynamic force*

Linear sloshing theory can better describe transient liquid sloshing on the time scale of the highest natural sloshing period T_1 than nearly resonant steady-state sloshing. In this section, we consider two cases of transient waves in a circular tank that are relevant during either a turning manoeuvre or a lane change of a tanker vehicle. Rollover is not considered, i.e. the tank experiences only the effect of horizontal accelerations $\ddot{\eta}_2(t)$, as illustrated in figure 7.

The horizontal hydrodynamic force $F_2(t)$ due to transient sloshing is investigated. An estimate of this transient force can be obtained by using fourth-order Runge–Kutta integration of the modal equations (2.9) with $\ddot{\eta}_2(t)$ represented in figure 7 and the zero-initial conditions $\beta_i(0) = \dot{\beta}_i(0) = 0$. The Runge–Kutta solution should then be substituted into (2.18) to compute the hydrodynamic force. Following this path with input accelerations in figure 7 establishes fast convergence to the time-dependent $F_2(t)$ when increasing the number of the modal equations (2.9). Using the three to four modal equations of (2.9) responsible for antisymmetric modes stabilizes three to six significant figures for the output hydrodynamic force $F_2(t)$. One reason for this fast convergence is that the obtained multimodal solution is, for these transients, characterized by a clear dominant contribution of the lowest natural mode. Our

calculations will be compared with published CFD results. However, no estimates of numerical accuracy were provided in the publications.

4.2.1. *The turning manoeuvre*

We apply our linear multimodal solution to re-examine the case by Aliabadi *et al.* (2003), who employed a fully nonlinear, three-dimensional Navier–Stokes model for simulation of transient sloshing in a horizontal circular cylindrical tank and associated horizontal force. Both the gas and the liquid were assumed incompressible. Aliabadi *et al.* (2003) used the finite element method based on the stabilized-upwind/Petrov–Galerkin and pressure-stabilized/Petrov–Galerkin techniques; the volume-of-fluid method is used to capture the liquid–gas interface. In their numerical examples, the transient sloshing occurs due to a turning manoeuvre. The vehicle is assumed to follow a circular path of radius $R_r = 250$ m and constant speed $v_t = 10\ \mathrm{m\,s^{-1}}$. The tank is as a consequence exposed to a constant horizontal centrifugal acceleration $\ddot{\eta}_{2a} = v_t^2/R_r = 0.4\ (\mathrm{m\,s^{-2}}) = 0.0408 \times g$. The time behaviour of $\ddot{\eta}_2(t)$ is described in figure 8(*a*) with $T_d = 0$. Zero-initial conditions for the liquid implying an unperturbed liquid at $t = 0$ are adopted.

Comparison of the simulations by Aliabadi *et al.* (2003) and the multimodal solution is presented in figure 8. Even though the simulations by Aliabadi *et al.* (2003) account for nonlinearity and viscosity, we see generally satisfactory agreement for all the tested liquid depths during an initial duration corresponding to the highest natural sloshing period $T_1 = 2\pi/\sigma_1$, namely, in the interval $0 < t\pi/\sigma_1 < 2$. In figure 8(*a*,*b*) with lower liquid depth, the simulations by Aliabadi *et al.* (2003) and our multimodal solution are in good agreement during the completely studied time interval $0 < t\pi/\sigma_1 < 5$. However, a clear discrepancy is established for the middle liquid depths (the middle liquid depths are classified in the supplementary material to be $0.8 \lesssim h/R_0 \lesssim 1.2$) in figure 8(*c*,*d*) when $2 < t\pi/\sigma_1$.

Because the lowest natural sloshing mode is clearly dominant in the multimodal solution for figure 8(*a–d*), the resulting oscillation period of the horizontal force is very close to the highest sloshing period T_1. The simulations by Aliabadi *et al.* (2003) for figure 8(*c*,*d*) associated with the middle liquid depths do not show the same periodicity. This implicitly indicates that higher natural modes become amplified in these simulations; an explicit confirmation of this fact follows from Aliabadi *et al.* (2003, figure 5) presenting an instant wave profile related to figure 8(*d*) which shows that the lowest natural mode does not dominate in their numerical solution. Typical mechanisms of such an amplification of higher modes is the free-surface nonlinearity (see Faltinsen & Timokha 2009, chapters 8 and 9).

4.2.2. *Lane change*

Fully nonlinear and viscous simulation of liquid sloshing due to the lane change manoeuvre of a tanker vehicle (figure 7*b*) was done by Moderassi-Tehrani *et al.* (2006) by using the commercial CFD code FLUENT. The numerical results were obtained for a two-dimensional tank of radius $R_0 = 1.0161$ m and the dimensional horizontal forcing acceleration amplitude $0.2 \times g$.

The multimodal solution and the numerical results by Moderassi-Tehrani *et al.* (2006) for maximum horizontal hydrodynamic force are compared in figure 9 for different ratios between the lane change duration T_d and T_1. One can see satisfactory agreement. Once again, as in § 4.2.1 for the turning-tanker vehicle, the multimodal solution demonstrates a clearly dominant contribution of the lowest natural mode; a

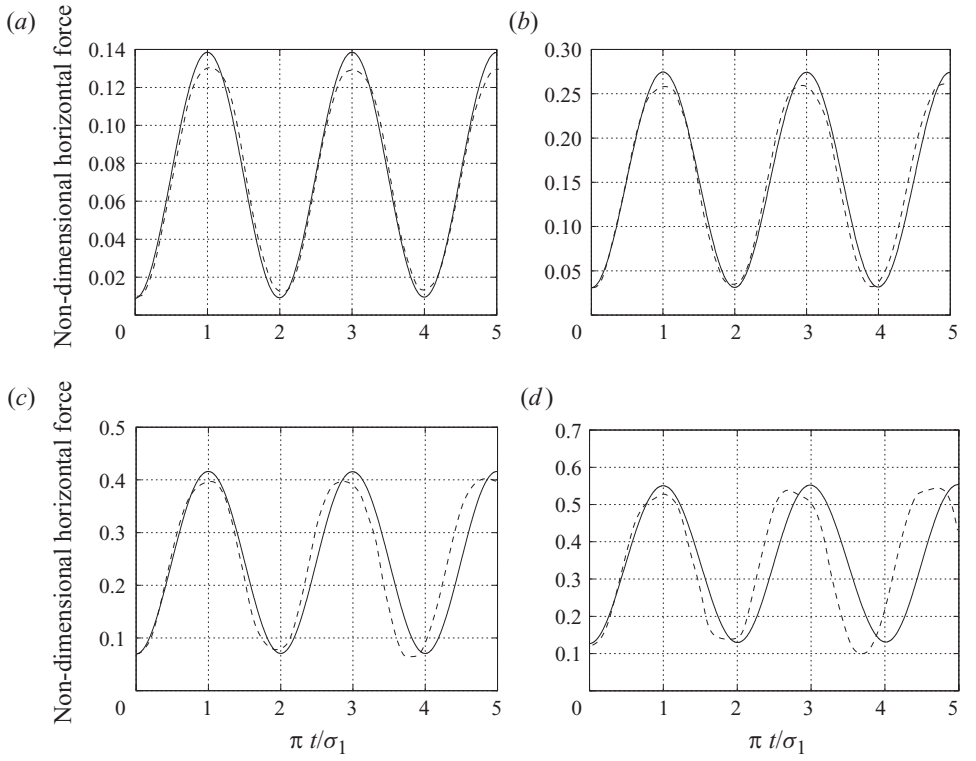

FIGURE 8. Non-dimensional horizontal force $F_2(t)/(\rho L_1(2R_0)^2\ddot{\eta}_{2a})$ for the turning manoeuvre of a tanker vehicle considered by Aliabadi *et al.* (2003), whose simulations (dashed line) were done with $2R_0 = 1$ m by a fully nonlinear, three-dimensional and viscous CFD model with $2R_0 = 1$ m as well as $T_d = 0$ and $\ddot{\eta}_{2a} = 0.0408g$ in the notation of figure 7(*a*); L_1 is the longitudinal dimension of the horizontal tank. The solid lines represent results by the linear multimodal theory. (*a*) $h/R_0 = 0.3$, (*b*) $h/R_0 = 0.5$, (*c*) $h/R_0 = 0.7$ and (*d*) $h/R_0 = 0.9$.

modal analysis shows that other modes give only a 2 % correction of the maximum value of $F_2(t)$.

FLUENT predicts lower values of the maximum horizontal force than the multimodal solution in a neighbourhood of $T_d/T_1 = 1$. The maximum discrepancy through all the compared values in figure 9(*b–d*) is about 15 %. An indication that this discrepancy is caused by the free-surface nonlinearity follows from comparing the hydrodynamic forces predicted by the nonlinear multimodal theory by Faltinsen *et al.* (2000) and the corresponding linear modal equations (Faltinsen & Timokha 2009) for a rectangularly shaped tank with the tank breadth $2R_0$, the liquid-depth-to-R_0 values taken from figure 9, and the same forcing conditions as in figure 9(*b–d*). The established maximum difference between the nonlinear and linear forces due to transient sloshing in this rectangular tank is estimated to being about the same 15 %.

5. Concluding remarks and discussion

Being motivated in developing the multimodal methods for forced oscillations of a horizontal circular cylindrical tank, we have constructed approximate natural sloshing modes in a two-dimensional circular tank. These analytically given modes exactly satisfy the Laplace equation, the zero-Neumann boundary conditions on the

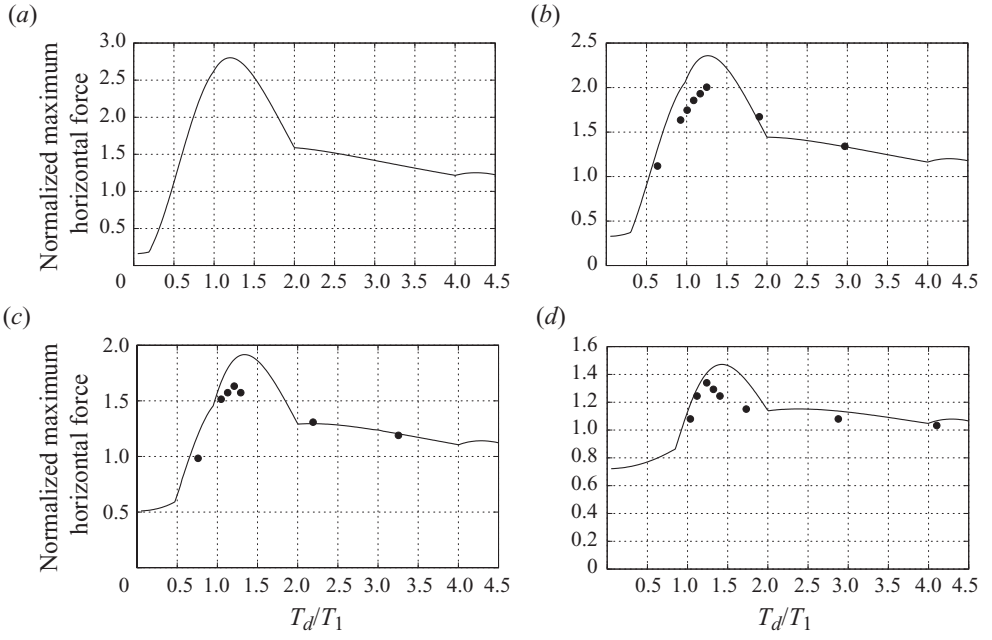

FIGURE 9. Non-dimensional maximum horizontal force $\max|F_2(t)|/(M_l\ddot{\eta}_{2a})$ for the lane change of a tanker vehicle, where $\ddot{\eta}_{2a}$ is the maximum acceleration in figure 7(*b*) and M_l is the liquid mass. The circles correspond to fully nonlinear viscous simulations by Moderassi-Tehrani *et al.* (2006) employing the FLUENT code, the solid lines are predictions by our linear multimodal solution. The simulations by Moderassi-Tehrani *et al.* (2006) were performed with $\ddot{\eta}_{2a} = 0.2g$, where $R_0 = 1.016$ m. (*a*) $h/R_0 = 0.4$, (*b*) $h/R_0 = 0.8$, (*c*) $h/R_0 = 1.2$ and (*d*) $h/R_0 = 1.6$.

wetted walls, and demonstrates a uniform convergence to the spectral free-surface condition. They capture the asymptotic behaviour at the corner points between the mean free surface and the non-vertical tank walls, which becomes singular as $h/R \geqslant 1$.

The natural sloshing modes are employed in the multimodal solution describing the linear forced sloshing problem in a circular two-dimensional tank (transverse forced waves in a horizontal circular cylindrical tank). The associated multimodal expressions for the hydrodynamic force were also derived. The constructed natural modes were adopted in computations of the hydrodynamic coefficients of the above-mentioned equations and expressions. Non-dimensional values of these coefficients are listed for $0.1 \leqslant h/R_0 \leqslant 1.95$. Linear viscous damping rates due to laminar flow at the tank surface were obtained by using the technique of Keulegan (1959).

Linear sloshing theory is commonly used in studying the forced liquid sloshing in a horizontal circular cylindrical tank (see a recent review by Karamanos *et al.* 2009). Because the constructed multimodal solution for forced sloshing is quite accurate, it is used to estimate the applicability of linear sloshing theory for steady-state and transient liquid motions. For this purpose, the solution is compared with experimental results and fully nonlinear CFD simulations. There is good consistency for non-resonant steady-state regimes and transients. For transient waves, the multimodal solution demonstrates a clearly-dominant contribution of the lowest (antisymmetric) natural mode. The agreement with published nonlinear CFD results is especially good for smaller liquid depths; however, the linear theory may lead to sufficient discrepancy

for larger tank fillings due to, we believe, the free-surface nonlinearity. We give some arguments for this.

Explicitly, the nonlinear effects appearing as overturning waves are confirmed in photographs by Kobayashi *et al.* (1989), who studied steady-state resonant sloshing due to horizontal tank excitations with relatively large forcing amplitude $0.01 \lesssim \eta_{2a}/R_0$. Furthermore, an explanation why the free-surface nonlinearity can become more important for larger tank fillings comes from the free-surface profiles associated with the lowest natural modes. For lower liquid depths, $h/R_0 \lesssim 0.8$, these profiles are characterized by almost linear behaviour as a function of the horizontal coordinate. Increasing the liquid depth leads to relatively steep-wave profiles at the tank wall. Remembering that the nonlinear free-surface condition involves derivatives of the velocity potential, this steepness indicates importance of the nonlinear terms for higher liquid depths. The fact that there is a geometrical conflict for the instant linear-theory free-surface profiles at the intersection point between the mean free surface and the tank wall also introduces nonlinear effects.

Faltinsen & Timokha (2009) review the asymptotic multimodal methods which effectively describe nonlinear forced liquid sloshing. Based on the natural sloshing modes from the present paper, these methods have no formal mathematical obstacles to be applied. The corresponding nonlinear multimodal equations should be of an adaptive character (adaptive multimodal methods for a rectangular tank are extensively discussed by Faltinsen & Timokha 2001). One reason is secondary resonance. Occurrence of the secondary resonance can be illustrated by jumps in the steady-state response curves seen in experimental measurements by Bogomaz & Sirota (2002) (see figure 6).

The nonlinear secondary resonance phenomenon occurs when both $\sigma \approx \sigma_1$ and the $n\sigma$-harmonics (n is an integer) are close to a higher natural sloshing frequency. For the rectangular tank, due to the trigonometric algebra between the natural sloshing modes, the n-harmonics should primarily cause the secondary resonance of the nth natural mode, i.e. one should estimate the closeness of $n\sigma$ and σ_n. The natural modes for the circular tank shape do not guarantee that the $n\sigma$-harmonics primarily amplify the nth mode. More precisely, for the second-order nonlinearities, we can expect the secondary resonance to excite *all* the symmetric modes, namely, one must estimate the closeness of 2σ and σ_{2j}, $j = 1, 2, \ldots$. In a similar way, the third-order nonlinearity requires us to control the condition $3\sigma \approx \sigma_{2j+1}$, $j = 1, 2, \ldots$. In terms of the ratio σ/σ_1, the secondary resonance due to the second-order nonlinearities should be expected at

$$\frac{\sigma}{\sigma_1} \approx i_{2j}^{(2)} = \frac{1}{2}\sqrt{\frac{\bar{\kappa}_{2j}}{\bar{\kappa}_1}}, \quad i = 1, 2, \ldots \tag{5.1}$$

and the secondary resonance due to the third-order nonlinearities at

$$\frac{\sigma}{\sigma_1} \approx i_{2j+1}^{(3)} = \frac{1}{3}\sqrt{\frac{\bar{\kappa}_{2j+1}}{\bar{\kappa}_1}}, \quad i = 1, 2, \ldots. \tag{5.2}$$

For the experimental case studied by Bogomaz & Sirota (2002), many of $i_k^{(2)}$ and $i_k^{(3)}$ belong to the primary resonance frequency range. These are marked in figure 6 and, as one can see, there are jumps at these values in the experimental measurements.

Finally, a prospective problem is the study of the passage from two-dimensional to three-dimensional waves in a horizontal circular cylinder due to horizontal excitations as observed in the experiments by Bogomaz & Sirota (2002).

Supplementary data are available at journals.cambridge.org/flm.

REFERENCES

Aliabadi, S., Johnson, A. & Abedi, J. 2003 Comparison of finite element and pendulum models for simulating of sloshing. *Comput. Fluids* **32**, 535–545.

Bogomaz, G. I. & Sirota, S. A. 2002 *Oscillations of a Liquid in Containers: Methods and Results of Experimental Studies* (in Russian). National Space Agency of Ukraine.

Djavareshkian, M. H. & Khalili, M. 2006 Simulation of sloshing with the volume of fluid method. *Fluid Dyn. Mater. Process.* **2** (4), 299–307.

Eastham, M. 1962 An eigenvalue problem with the parameter in the boundary condition. *Q. J. Math.* **13**, 304–320.

Faltinsen, O. M., Rognebakke, O. F., Lukovsky, I. A. & Timokha, A. N. 2000 Multidimensional modal analysis of nonlinear sloshing in a rectangular tank with finite water depth. *J. Fluid Mech.* **407**, 201–234.

Faltinsen, O. M. & Timokha, A. N. 2001 Adaptive multimodal approach to nonlinear sloshing in a rectangular tank. *J. Fluid Mech.* **432**, 167–200.

Faltinsen, O. M. & Timokha, A. N. 2009 *Sloshing*. Cambridge University Press.

Karamanos, S. A., Papaprokopiou, D. & Platyrrachos, M. A. 2009 Finite element analysis of externally-induced sloshing in horizontal-cylindrical and axisymmetric liquid vessels. *J. Press. Vessel Technol.* **131**, 051301.

Keulegan, G. 1959 Energy dissipation in standing waves in rectangular basins. *J. Fluid Mech.* **6** (1), 33–50.

Kobayashi, N., Mieda, T., Shiba, H. & Shinozaki, Y. 1989 A study of the liquid slosh response in horizontal cylindrical tanks. *Trans. ASME J. Press. Vessel Technol.* **111**, 32–38.

Komarenko, A. 1980 Asymptotic expansion of eigenfunctions of a problem with a parameter in the boundary conditions in a neighborhood of angular boundary points. *Ukrainian Math. J.* **32** (5), 433–437.

Kulczycki, T. & Kuznetsov, N. 2009 'High spots' theorems for sloshing problems. *Bull. Lond. Math. Soc.* **41**, 495–505.

Lukovsky, I. A. 1990 *Introduction to Nonlinear Dynamics of Rigid Bodies with the Cavities Partially Filled by a Fluid* (in Russian). Naukova Dumka.

Lukovsky, I. A., Barnyak, M. Y. & Komarenko, A. N. 1984 *Approximate Methods of Solving the Problems of the Dynamics of a Limited Liquid Volume* (in Russian). Naukova Dumka.

McIver, P. 1989 Sloshing frequencies for cylindrical and spherical containers filled to an arbitrary depth. *J. Fluid Mech.* **201**, 243–257.

Moderassi-Tehrani, K., Rakheja, S. & Sedaghati, R. 2006 Analysis of the overturning moment caused by transient liquid slosh inside a partly filled moving tank. *Proc. Inst. Mech. Engrs, Part D: J. Automob. Engng* **220**, 289–301.

Morand, J.-P. & Ohayon, R. 1995 *Fluid Structure Interaction: Applied Numerical Methods*. Wiley.

Navarrete, J. A. R., Cano, O. R., Romero, J. M. F., Hildebrand, R. & Madrid, M. M. 2003 Caracterización experimental del oleaje en tanques. *Tech. Rep.* 219. Instituto Mexicano del Transporte (IMT), Secretaria de Comunicaciones Y Transportes (SCT).

Strandberg, L. 1978 Lateral sloshing of road tankers, vol. 1: main report. *Tech. Rep.* 138A-1978. National Road & Traffic Research Institute, S-58101, Linköping, Sweden.

Vekua, I. N. 1953 On completeness of a system of harmonic polynomials in space. *Doklady Akad. Nauk SSSR (NS)* **90**, 495–498.

Vekua, I. N. 1967 *New Methods for Solving Elliptic Equations*. Wiley.

Wigley, N. M. 1964 Asymptotic expansions at a corner of solutions of mixed boundary value problems. *J. Math. Mech.* **13**, 549–576.